Deep–Sea Research I 179 (2022) 103666

Contents lists available at ScienceDirect

Deep-Sea Research Part I

journal homepage: www.elsevier.com/locate/dsri

Research Paper

Surface wave height regulated by ocean currents: An observational perspective

Tianyi Cheng [a,b], Zhaohui Chen [a,b,*], Jingkai Li [a,b], Xin Ma [a,b], Qi Wen [c], Lixin Wu [a,b]

[a] Physical Oceanography Laboratory/Institute for Advanced Ocean Science/Frontiers Science Center for Deep Ocean Multispheres and Earth System, Ocean University of China, Qingdao, China
[b] Qingdao National Laboratory for Marine Science and Technology, Qingdao, China
[c] College of Information Science and Engineering, Ocean University of China, Qingdao, China

ARTICLE INFO

Keywords:
Significant wave height
Current effects on waves
Drifting wave buoy
Kuroshio extension

ABSTRACT

Ocean currents exert notable influences on surface wave height through wave-current coupling. In this paper, we provide solid evidences that ocean currents can regulate the significant wave height (SWH) by comparing measurements of a fleet of surface drifting wave buoys (DrWBs) with GFS-WW3 model product. In the Kuroshio Extension (KE) of Northwestern Pacific, the SWH observed by DrWBs are shown to be generally lower (higher) than that simulated by GFS-WW3 when waves propagate towards (against) the direction of surface currents. It is indicated that the GFS-WW3 product could be underestimated/overestimated by up to 5% compared with observed SWH if the forcing from current field is not involved. Adopting altimeter derived data, further analysis shows consistent relationship between observed and modelled SWH in the global ocean, except for regions where ocean swells dominate. The findings may help improve wave model simulations without increasing computational burdens if this relationship is considered.

1. Introduction

Longuet-Higgins and Stewart (1961, 1962) proposed that waves and ocean currents were coupled by wave-induced radiation stress, and the nonlinear interaction between waves and currents would influence the wave amplitude and current velocity. In the following decades, the theories of wave-current interactions were continuously developed and established. On one hand, ocean currents do work on waves indirectly through modifying the effective wind speeds at ocean surface (Ardhuin et al., 2012) or directly modifying wave frequency through Doppler shift (Villas Bôas et al., 2020), which may lead to wave refraction, and change the wave amplitude, wavelength and steepness, thus resulting in wave breaking (Peregrine, 1976). On the other hand, waves act on ocean currents as well through Stokes drift (Kenyon, 1969), which is considered responsible for the Langmuir circulation by interacting with wind-driven currents (Craik and Leibovich 1976; McWilliams et al., 1997). Besides, surface waves affect the surface roughness and resultant wind stresses, thus exert influences on wind-driven currents (Donelan et al., 1993).

Effects of ocean currents on waves have been extensively studied through remote sensing and numerical modeling approaches. Most of these studies focused on regions of strong ocean currents like the Gulf Stream (Meadows et al., 1983; Mapp et al., 1985; McLeish and Ross, 1985; Liu et al., 1989; Wang et al., 1994; Melville et al., 2005; Haus, 2007; Romero et al., 2017), Kuroshio and Agulhas currents where *in-situ* wave observations are frequently conducted (Irvine and Tilley, 1989; Lavrenov, 1998; Hwang, 2005; Quilfen and Chapron, 2019). By means of remote sensing, previous studies have come to the preliminary conclusions that the influence of strong ocean currents will cause enhancement/reduction in wave heights (Liu et al., 1989; Hwang, 2005).

With respective to modelling studies, it has been possible to have in-depth investigations into wave-current interactions. In recent two decades, the current-induced effects on waves have been assessed using not only stand-alone third-generation wave models, but also current-wave coupling ocean models (Holthuijsen and Tolman, 1991; Wang et al., 1994, 2020; Xie et al., 2001; Tamura et al., 2008; Fan et al., 2009; Warner et al., 2010; Ardhuin et al., 2017). For example, using a coupled atmosphere-ocean-wave model, Jensen et al. (2011) proposed a relationship that the wave-current interaction results in higher significant wave height (SWH) as the waves run against the Florida current, and

* Corresponding author. Physical Oceanography Laboratory/Institute for Advanced Ocean Science/Frontiers Science Center for Deep Ocean Multispheres and Earth System, Ocean University of China, Qingdao, China.
E-mail address: chenzhaohui@ouc.edu.cn (Z. Chen).

https://doi.org/10.1016/j.dsr.2021.103666
Received 2 May 2021; Received in revised form 7 September 2021; Accepted 3 November 2021
Available online 12 November 2021

vice versa as they run toward the Florida current. A recent modelling study by Wang et al. (2020) suggested that the influence of the wave-current interactions on wave height in the Kuroshio region was about 10–20%.

In addition to the western boundary current regions, there have been numerous modelling studies associated with the effects of currents on waves in some semi-enclosed or marginal seas such as the Adriatic Sea, the North Sea, and the Yellow Sea of China (Osuna and Monbaliu, 2004; Moon, 2005; Benetazzo et al., 2013; Barbariol et al., 2013). For those semi-enclosed and marginal seas where tidal currents are strong, the impacts of currents on waves were observed as well. Using a current-wave coupled model, Osuna and Monbaliu (2004) illustrated that the effect of coupling on SWH is about 3%. Other modellings studies have also reached cognitions that incorporating the coupling between waves and currents can reduce errors compared with observations (Ardhuin et al., 2012; Benetazzo et al., 2013).

Most of the studies, as mentioned above, mainly focus on wave-current interactions either in strong western boundary currents or tidal currents dominant regions, yet the effects of currents on waves are not conclusively addressed from a global ocean perspective. In the mid-latitude ocean such as western boundary current extensions and Antarctic Circumpolar Current (ACC) regions where strong oceanic eddies and atmospheric storms are dominant, though covered by plenty of remote sensing data (Quilfen and Chapron, 2019), there are few *in-situ* observations regarding the ocean currents and waves under harsh sea conditions. Therefore, it is required to have more observational evidences in those regions to facilitate our understandings on this issue.

In this study, we analyzed a fleet of newly developed drifting wave buoys (DrWBs, hereinafter wave buoys for brevity) deployed in the Kuroshio Extension (KE), one of the most dynamically-complex regions in the global ocean, to assess the surface current effects on ocean wave height in detail. Then, we expanded the findings to a global scale by analyzing the altimeter data. In particular, we aim to assess how much wave height is missing for a widely-used wave model product in which the wave-current interactions are not considered. The rest of this paper is organized as follow: section 2 introduces the wave buoys with the data retrieved and the methods of data analysis; detailed results including the wave height comparison with numerical model product, relationship of observation-model differences with wave/current directions, and global view of current-induced wave height deviation are described in section 3; mechanisms of ocean current effect on wave height are discussed in section 4; followed by conclusions in section 5.

2. Data and methods

2.1. Data

The drifting wave buoys used in this study are newly developed light-weighted mini-buoys that can measure the wave height and period in drifting way. Technically, the wave buoy employs a nine-component acceleration sensor and transmits the processed data via Iridium/Beidou/4G/short-wave communications simultaneously. The nine components by the accelerometer inside the buoy are collected, and the quadratic integration of acceleration is taken as the elevation of water particle. The low-frequency noise is reduced by removing the trend after twice integrations during data processing and the statistical wave parameters like SWH are sent back by calculating the first 10-min samplings. Detailed information of the data processing can be found in the supplementary information (SI) of this paper.

With a diameter of 40 cm and a total weight of 11 kg (Fig. S1), the wave buoy is of easy deployment and suitable for fast *in-situ* wave observations for multiple needs. The power of the wave buoy can last for 180 days in normal working mode. To verify the performance of the wave buoy, we conducted a 15-day field comparison test with a Waverider buoy made by Dutch DataWell MKIII off the Qingdao coast. For most sea states, the SWH and mean wave period obtained from two buoys show a good consistency (Fig. 1a&b), with *RMSE* being 0.08 m and 0.37 s, respectively. A closer look at the frequency spectrum (Fig. 1c&d) shows a good correspondence between Waverider and wave buoy, and no obvious spurious resonance is found in the spectrum. Generally, this kind of wave buoys are capable of estimating wave parameters and are competent with *in-situ* observations in open oceans.

The *in-situ* observations of SWH used in this study was derived from 16 wave buoys deployed in 2019 and 2020 in Northwest Pacific Ocean (see details in Table 1) and these buoys were largely centered in the KE region (Fig. 2a). Besides, we applied the Jason-3 Geophysical Data Records (GDRs) along-track SWH and the daily gridded SWH of $1^\circ \times 1^\circ$ resolution by merged satellite altimeters of Jason-3, Sentinel-3A and SARAL/Altika, both of which are provided by Archiving, Validation, and Interpretation of Satellite Data in Oceanography (AVISO). The modelled wave parameters used in this study are the hourly wave height and peak wave direction with 0.5° spatial resolution from the third-generation wave model WAVEWATCH III (WW3) forced by NOAA-NCEP's Global Forecast System (GFS) winds with 0.5 arc-degree spatial resolution in hourly intervals. This model product is designed to capture the large-scale ocean waves and distributed by the Pacific Islands Ocean Observing System.

To illustrate ocean current effects on wave height, we use 3-hourly ocean surface currents derived from the global surface $1/12^\circ$ product of Hybrid Coordinate Ocean Model (HYCOM), together with the daily satellite product MULTIOBS_GLO_PHY_REP_015_004 (Rio et al., 2014) provided by Copernicus-Marine environment monitoring service (CMEMS). The satellite-based velocity fields are obtained by combining CMEMS reprocessed satellite geostrophic surface currents and modelled Ekman currents at the sea surface. Besides, surface velocity can also be estimated by wave buoys' trajectories in consideration of negligible effect on the wave buoy by direct wind force (Guimarães et al., 2018), and they show good consistency in representing the surface currents comparing with HYCOM and CMEMS (Fig. S2).

2.2. Difference between simulation and observation (D)

To compare the observed SWH by wave buoys with the GFS-WW3 product, we linearly interpolated the gridded data onto the location and observing time of each wave buoy. Frist, we calculated the overall error between GFS-WW3 simulated SWH and observed SWH, which is represented by the bias between simulations and observations as follows:

$$BIAS = \frac{1}{n}\sum_{i=1}^{n}(H_{mi} - H_{oi}) \quad (1)$$

where H_{mi} is the GFS-WW3 simulated SWH, H_{oi} is the observed SWH by wave buoys, the subscript i denotes each observing point with different locations and times, and n is the total number of observations. It is shown in Fig. 2b that the simulated SWH is generally consistent with observations by analyzing all 32609 data pairs, with a high correlation coefficient of 0.93. Detailed statistical examinations of simulated and observed SWH indicate that the mean SWH derived from the GFS-WW3 model (~3.0 m) is approximately 0.2 m higher than the observations (~2.8 m).

The apparent overestimated *BIAS* between model and observations are possibly caused by various reasons. For example, there may be systematic errors in the measurement of wave height by the wave buoys, and/or the model results from WW3 may generally higher in connection with the relatively stronger GFS winds (Carracedo García et al., 2005; Stopa and Cheung, 2014; Campos et al., 2021). Since our focus of this study is examining the effect of ocean currents on wave height, as will be shown later, the presence of mean deviation between model and observation does not resultantly change the conclusions. In the rest of this study, therefore, we define D and P as the difference and relative difference between simulations and observations, respectively.

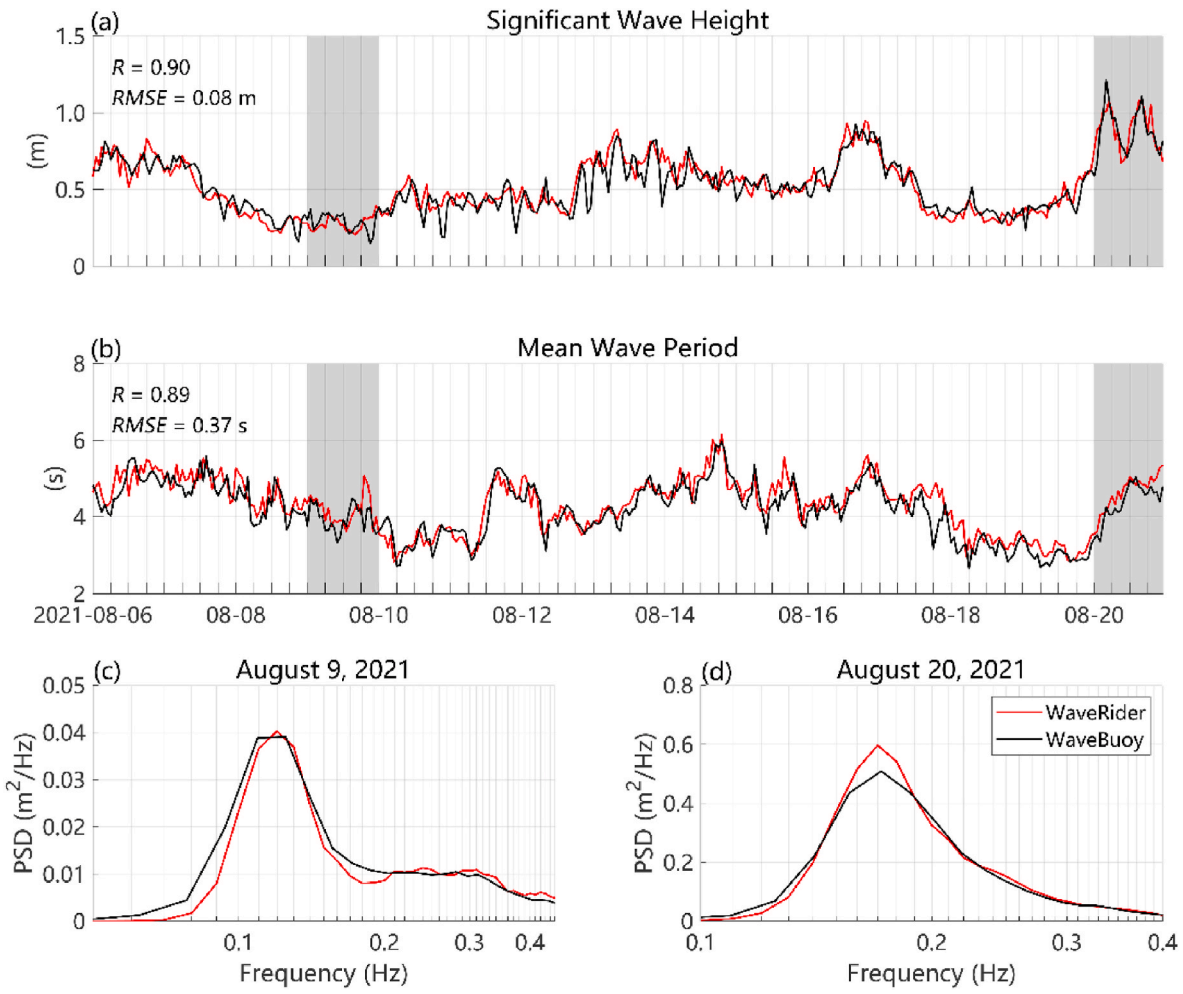

Fig. 1. Comparison of the integrated wave parameters and wave power spectral density (PSD) estimate from Datawell Waverider and drifting wave buoy. (a) Significant wave height. (b) Mean wave period. (c–d) Wave PSD for a single day of calm sea state (August 9, 2021) and another single day of relatively harsh sea state (August 20, 2021), respectively. These two days are denoted with shadings in (a) and (b). Correlation coefficient (*R*) and root mean square error (*RMSE*) are marked in both (a) and (b).

Table 1
Details of 16 drifting wave buoys.

ID	Date of deployment	Location of deployment	Duration (days)
WB161	September 3, 2019	144.6°E, 32.4°N	237
WB162	September 6, 2019	149.3°E, 39.0°N	10
WB164	September 8, 2019	154.4°E, 37.6°N	20
WB165		152.9°E, 37.6°N	230
WB166		153.4°E, 37.6°N	233
WB167		153.9°E, 37.6°N	233
WB168		152.0°E, 37.6°N	40
WB169		152.5°E, 37.6°N	37
WB133	November 10, 2019	150.0°E, 35.0°N	75
WB134	November 8, 2019	150.0°E, 40.0°N	50
WB136	November 13, 2019	150.0°E, 28.0°N	107
WB137	November 18, 2019	150.0°E, 13.0°N	46
WB181	June 17, 2020	149.3°E, 39.0°N	76
WB182			
WB183	June 21, 2020	146.7°E, 35.0°N	72
WB186			

Regardless of the mean deviation, D is defined as follows:

$$D_i = H_{mi} - H_{oi} - BIAS \tag{2}$$

and P is defined as follows:

$$P_i = \frac{D_i}{H_{oi}} \times 100\% \tag{3}$$

In addition, we defined A as the angle between the directions of wave and current, which ranges from 0° (same direction) to 180° (opposite direction).

A statistical parameter, i.e., correlation coefficient (R) and a statistical method, i.e., linear least squares regression fit are used to determine the relationship between D (P) and A. Here R can be defined as:

$$R = \frac{\frac{1}{n}\sum_{i=1}^{n}\left(A_i - \overline{A}\right)\left(D_i - \overline{D}\right)}{\sqrt{\frac{1}{n}\sum_{i=1}^{n}\left(A_i - \overline{A}\right)^2}\sqrt{\frac{1}{n}\sum_{i=1}^{n}\left(D_i - \overline{D}\right)^2}} \tag{4}$$

In order to avoid the influence of sampling on statistical results, we randomly selected half of the total number of data pairs and conducted the statistical process repeatedly, and the results did not change substantially.

3. Current effects on wave height

3.1. Regional view in the Northwest Pacific Ocean

Fig. 2b shows a good consistency between the observed and simulated SWH in the Northwest Pacific Ocean. However, a careful

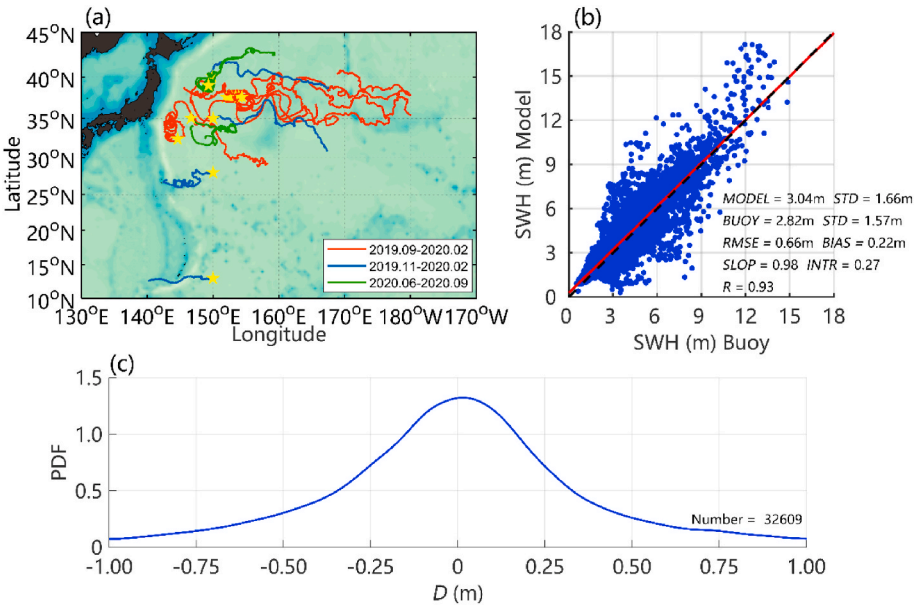

Fig. 2. (a) Trajectories of 16 wave buoys deployed in the Northwest Pacific Ocean in September 2019 (red), November 2019 (blue), and June 2020 (green), respectively. The yellow stars denote the locations of wave buoy deployment. (b) Scatter plot of hourly SWH derived from the observations and GFS-WW3 product with statistics labeled. *MODEL/BUOY*: mean SWH of GFS-WW3/wave buoys. *STD*: standard deviation. *RMSE*: root mean square error. *SLOP/INTR*: slope/intercept of the linear regression. (c) Probability density function (PDF) of *D*.

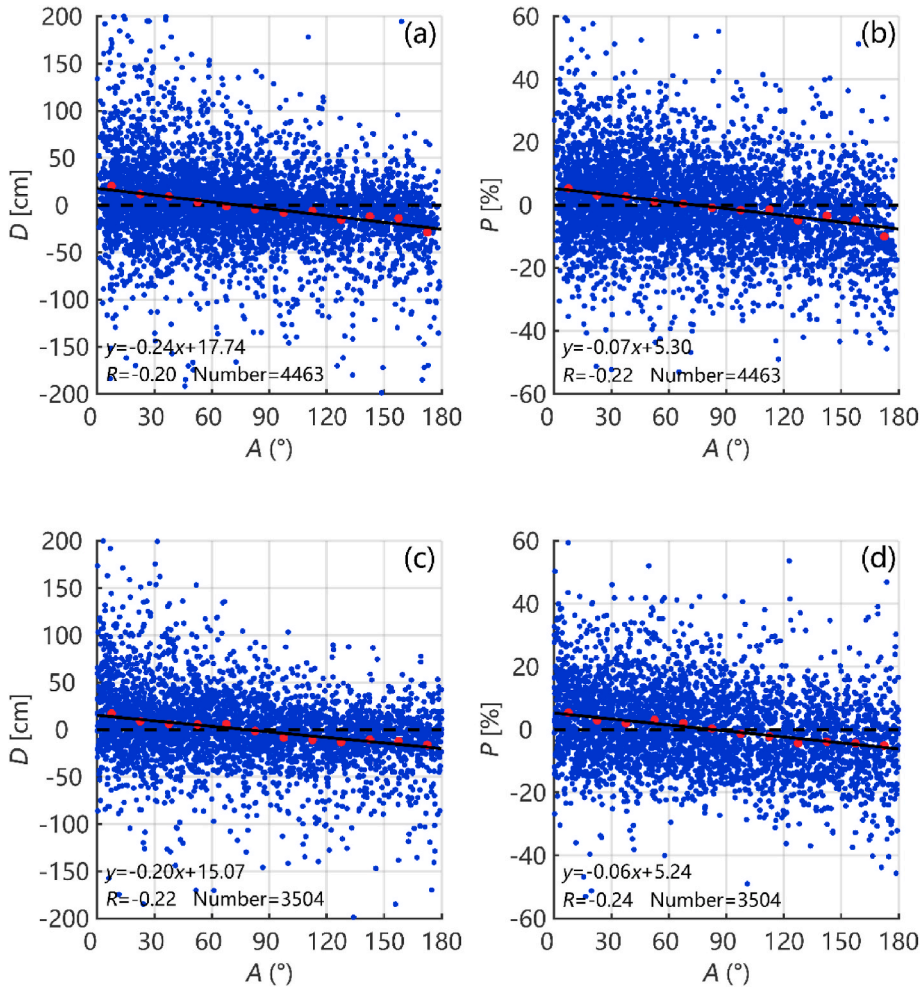

Fig. 3. *D* and *P* as a function of *A*. The red dots denote bin-averaged values for each 15° bin and the solid line is the linear fit. The linear regression equation, correlation coefficient *R*, and the number of points are indicated. The derivation of wave and current relative direction *A* used surface currents derived from (a, b) HYCOM and from (c, d) wave buoys. The linear regression equations above have all passed the significance test with a confidence level of 95%.

examination on D show that there exist large deviations over meters in many cases (Fig. 2c). The distribution of probably density of D implies that the large deviations may not result from random errors, but some mechanisms implicitly expressed/missed by the wave model products. It should be emphasized that the wave-current interactions are not incorporated in this GFS-WW3 product, which may serve a potential candidate that contributes to the deviation between observations and simulations. In particular, the direction of ocean currents and waves have been recognized as an important factor that modulates the wave height, i.e., the wave height decreases when the waves are in the same direction as the currents ($A < 90°$) while increases as the waves are opposite to the currents ($A > 90°$) (Jensen et al., 2011; Benetazzo et al., 2013; Samiksha et al., 2017; Wang et al., 2020). In this regard, a linear regression of D on A is conducted to verify the role of wave/current directions on wave height based on the 16 wave buoys.

Numerical simulations have indicated that waves converge in the countercurrent region and diverge in the down-flow region (Wang et al., 2020). It is also the case, as shown in Fig. 3a, that the SWH in GFS-WW3 simulations are higher than observations when the waves and currents are in the same directions ($0° \leq A \leq 60°$), while it is lower when they are in the opposite directions ($120° \leq A \leq 180°$). The linear fit of all points is characterized by a negative slope, statistically depicting the relationship of wave height deviations D and angle A between wave and current. More specifically, when A is 0°, i.e., the directions are completely the same, on average the simulated SWH is expected to be 18 cm higher than the observed, which accounts for approximately 5%. On the contrary, the simulated SWH is 25 cm lower (about 7%) when waves and currents are completely in opposite directions (Fig. 3a & b).

It should be noted that the wave buoys did not output the wave direction, so that we have to adopt the wave direction from the GFS-WW3 simulations. As for surface current, we adopt both the HYCOM data and the data derived from buoy drift. The buoy drift at sea surface may be affected by wave induced current or directly forced by the wind, so the GPS-derived surface current may introduce errors. But these errors are of relative insignificance compared with background surface current, and further examinations using wave buoy derived currents indicate that it does not change the results substantially (Fig. 3c and d). In view of the influence of sampling on statistical results, we randomly selected half of the total number of data pairs and calculated the relationship between D and A. This process was repeated over 1000 times to ensure the reliability of the results. It is shown in Fig. 4 that, no matter what kind of surface current data we use, D and A are all negatively correlated, proving that the results are not affected by data sampling.

To further explore the influence of surface currents on wave height, we examined the relative difference P with a variety of background surface current speeds. It is demonstrated in Fig. 5a & c that when the waves and currents are generally in the same directions ($0° \leq A \leq 30°$), the slope of the linear fit is positive, indicating that the deviation of simulated SWH increases along with surface velocities. For the case of opposite directions ($150° \leq A \leq 180°$), on the contrary, it shows a more prominent negative trend (Fig. 5b & d). The above explicitly highlight the role of ocean surface currents on modulating the wave height, that is, the higher the ocean surface velocity is, the wave height will be more significantly modulated. The results are consistent with recent modelling studies by Wang et al. (2020) and observational studies by Hwang (2005) and Romero et al. (2017), who all showed the non-negligible role of wave-current interactions on the wave height.

As mentioned previously, most of the studies put emphasis on boundary current regions like Kuroshio and Gulf Stream. Note that most of the wave buoys reported here are in the eddy-rich KE region, which means the current effects on wave height modulation are expected to be significant. To further investigate whether the regulation of SWH by currents is consistent in other oceans, we expand our focus from regional to global perspective in the next part.

3.2. Global view

Compared with observations in the KE region, the simulated SWH from GFS-WW3 is shown to be higher when directions of wave and current are the same, while it is lower as their directions are opposite. In this regard, the modulation on wave height by surface current can be explicitly expressed by a negative slope of the regression equation. Due to the absence of wave-current interactions in the GFS-WW3 product, it is anticipated that the GFS-WW3 product should be characterized by the

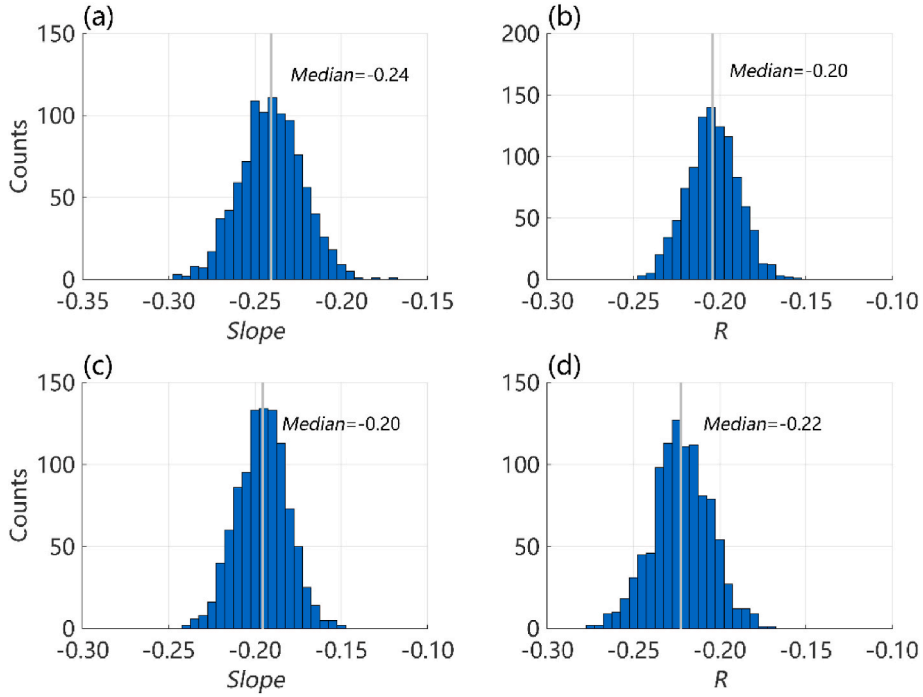

Fig. 4. Histograms of the *Slope* of linear regression and R between D and A. The *Median* value is indicated in grey line for each parameter. A is calculated based on the surface current from (a, b) HYCOM and (c, d) wave buoys. Counts are the number of times in 1000 trials that a certain *Slope* or R is corresponds to.

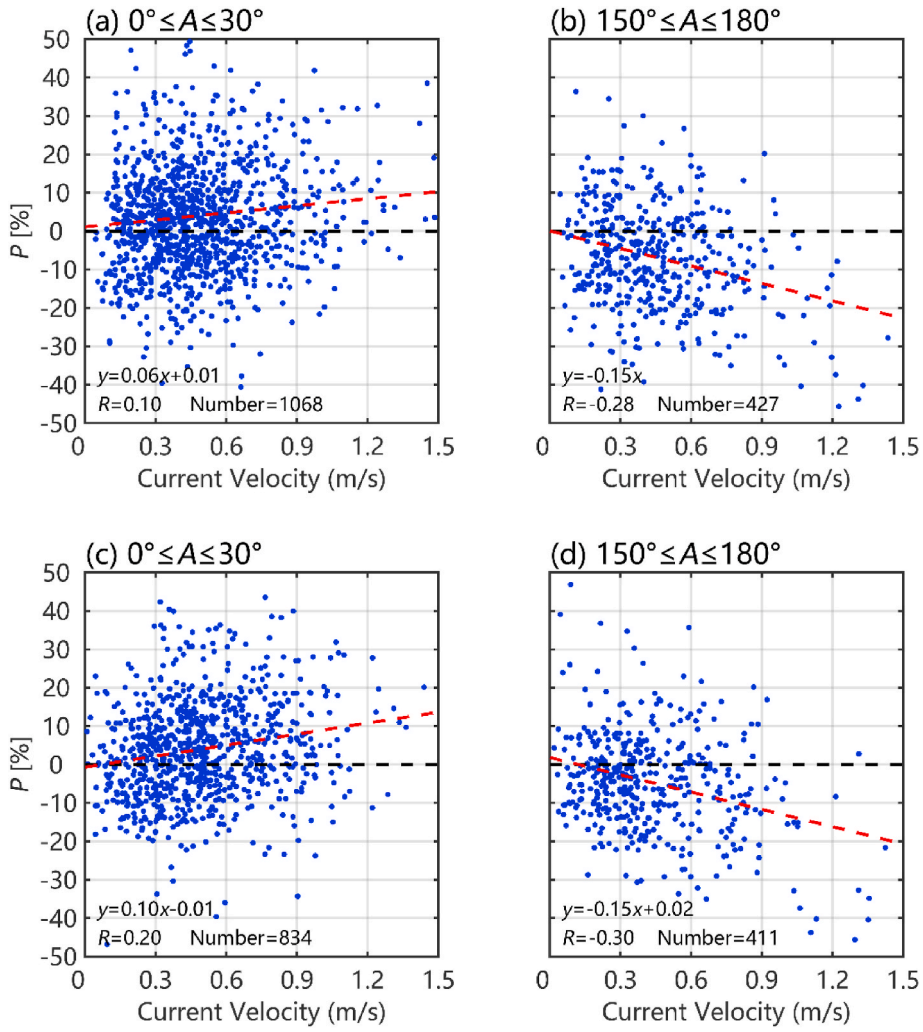

Fig. 5. *P* as a function of current speeds when (a, c) $0° \leq A \leq 30°$ and (b, d) $150° \leq A \leq 180°$. The red dashed line denotes the linear fit. The results are calculated based on currents of (a, b) HYCOM and from (c, d) wave buoys. The linear regression equations above have all passed the significance test with a confidence level of 95%.

similar pattern globally compared with observations.

Here, we adopt merged altimeters (Jason-3, Sentinel-3A and SARAL/Altika) observations of SWH, which cover the period from September 2009 to December 2019 and conduct comparisons with the GFS-WW3 product. Though the Sentinel-3A SWH may slightly larger than buoy observations, and differences between Altika and buoy measurements are larger for larger SWH values, both of the altimeters can meet the accuracy requirements and performs well in estimating the SWH (Kumar et al., 2015; Yang et al., 2019). In addition, the validation of SWHs derived by the Sentinel-3A and Jason-3 altimeters against buoy wave

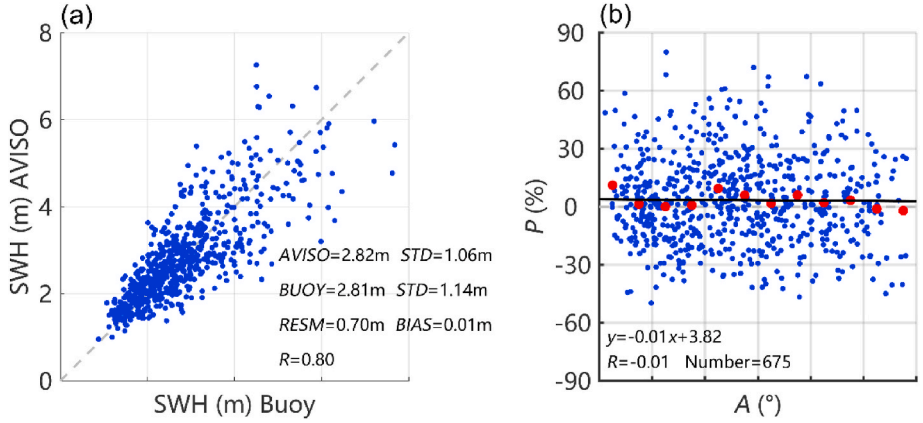

Fig. 6. Scatter plot of (a) daily mean SWH and (b) *P* as a function of *A*. Note that the linear regression in (b) does not pass the significance test with a confidence level of 95%.

data showed that the accuracy of the both satellites was temporally stable (Yang et al., 2020).

Our verification shows a good consistency between merged altimeter-derived SWH and the wave buoys with a little bit larger difference under high wave conditions (Fig. 6a). Unlike the above-mentioned results between GFS-WW3 model and wave buoys (Fig. 3), there seems no significant negative correlation between A and P that are derived from altimeters and wave buoys (Fig. 6b). The independence of P on A indicates that the altimeter-derived SWH, which is similar to wave buoys measurement, involves the full wave-current interaction processes in the real ocean. In this regard, we are confident to replace the wave buoys by altimeters to take a global view of surface currents regulation on the wave height.

In this section, the angle A with a bin of 10° between current and wave direction is calculated with two datasets of ocean current. One is derived from the HYCOM assimilations and the other one is CMEMS observations, while the GFS-WW3 product provides the peak wave directions. Here, P refers to the mean relative difference between GFS-WW3 simulations and satellite altimeter observations. Since our main focus is the open ocean, the regions where the depth is less than 2000 m and distance to the coast is less than 200 km, are all excluded in the subsequent statistics. It is demonstrated in Fig. 7 that the overall pattern of P along with A resembles what we have shown using the wave buoys, namely, the SWH by GFS-WW3 simulation is higher (lower) when the waves are in the same (opposite) direction as the surface currents, whatever the ocean currents datasets we use. From a global view, the simulated SWH is approximately 4% higher than altimetry measurement as waves propagate towards the direction of surface currents, while it is 5% lower as waves are against the ocean surface currents (Fig. 7). Given the strong temporal variability of the wave height, we repeated the analysis with Jason-3 along-track satellite data instead of the gridded AVISO SWH product, and the overall pattern remains unchanged (Fig. S3). Note that for the along-track data analysis, both the spatial and temporal resolution of wave parameters from GFS-WW3 (from 1° to 0.5°, daily to 3-hourly) and HYCOM current (from 1° to 1/12°, daily to 3-hourly) are improved, which may favor the reduction of the error range. In a word, the global average findings are consistent with the observational results using wave buoys in section 3.1.

To better illustrate the surface current effect on waves, we followed Plagge et al. (2012) and projected the surface velocities onto the direction of waves, which is defined as

$$u_p = |\boldsymbol{U}| \times \cos A \tag{5}$$

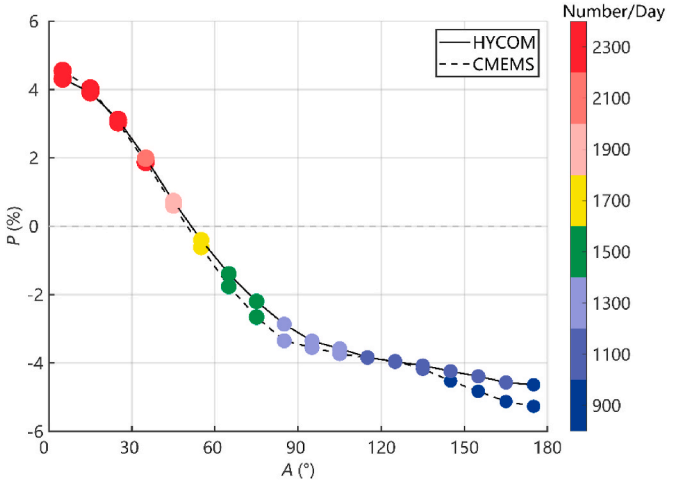

Fig. 7. Bin-averaged SWH relative difference (P) as a function of A using the ocean surface currents provided by HYCOM and CMEMS, respectively. The numbers denote the amount of data pairs into calculations.

where $|\boldsymbol{U}|$ is the surface current magnitude. Then we calculated the correlation coefficient R between SWH deviation and projected surface velocities (u_p). Different from what we have shown in section 3.1, this approach is more straightforward to depict the surface currents in terms of intensity and direction relative to waves. Note that a positive correlation coefficient is corresponding to the negative slope of the linear fit, which means the deviations of SWH between GFS-WW3 and altimeter wave observations are positively correlated with the projected velocities. In a word, as the waves and currents are in the same (opposite) direction, the projected velocities are positive (negative), and the GFS-WW3 simulated SWH is higher (lower) than observations. Thus, the correlation coefficient is always positive, implying the anticipated effect of surface currents on wave height.

We analyzed the daily output of SWH from AVISO and GFS-WW3, as well as the ocean surface currents provided by CMEMS from year 2011–2018. It is demonstrated in Fig. 8 that, in most of areas, the effect of surface currents on wave height is consistent with previous conclusions we have drawn in the KE region and global average. However, in the eastern basins of low-latitude ocean, where swells are significant (Chen et al., 2002), the deviation of wave height is negatively correlated with the projected velocities. It indicates that the direct effect of currents on waves is not that prominent in swell-dominant regions. On one hand, the direct current effect on wave height is inapparent in this region because the relatively weak surface current. On the other hand, it may be covered up by indirect influence of current-related relative wind effect.

4. Discussions on mechanisms of ocean current effect on wave height

There are several mechanisms that account for the current effect on waves. In this paper, we tend to highlight the effect of Doppler shift caused by ocean currents, which is expressed as the wave height difference depending on the difference between wave and current directions. It should be noted that the third-generation spectral wave models operate based on conservation of wave action. The wave action spectral density is expressed as $N = E/\sigma$, where E is the spectral energy density proportioned to the square of the significant wave height and σ is the wave radian frequency. Being identified as the intrinsic or relative frequency (as observed in a frame of reference moving with the mean current $\boldsymbol{U}$),

$$\sigma = \sqrt{gk \tanh kd} = \omega - \boldsymbol{k}\cdot\boldsymbol{U} \tag{6}$$

where d is the water depth, ω is the absolute frequency (as observed in a fixed frame) and $\boldsymbol{k}$ is the wave-number vector with magnitude k and direction θ (Tolman, 1991).

A consequence of wave action conservation (E/σ) can be understood as follows. If the absolute frequency ω keeps constant (Ardhuin et al., 2012), the wave propagating over ocean current will experience increase/decrease in its relative frequency σ and, consequently, the wave energy (wave height) will increase/decrease. Specifically, when the waves and currents propagate to the same direction, $\boldsymbol{k}\cdot\boldsymbol{U} > 0$, which results in a decrease of σ. Then the wave energy E decreases to maintain the conservation of N, which is manifested as the decrease of SWH. On the contrary, the SWH increases when waves and currents propagate to opposite directions ($\boldsymbol{k}\cdot\boldsymbol{U} < 0$). Further, the effects of ocean currents are absent in the GFS-WW3 model product we used here, so the model accuracy differs depending on the difference between wave and current directions can be understood in terms of this effect.

Besides, the relative wind effects, which can be interpreted as an indirect effect of the current on the waves, do work on wave height through modifying the effective wind speeds at ocean surface. Wind blowing over a surface in motion will produce a different stress on the water surface. For example, if winds and currents are running in the same direction, the momentum flux to the waves is reduced and the

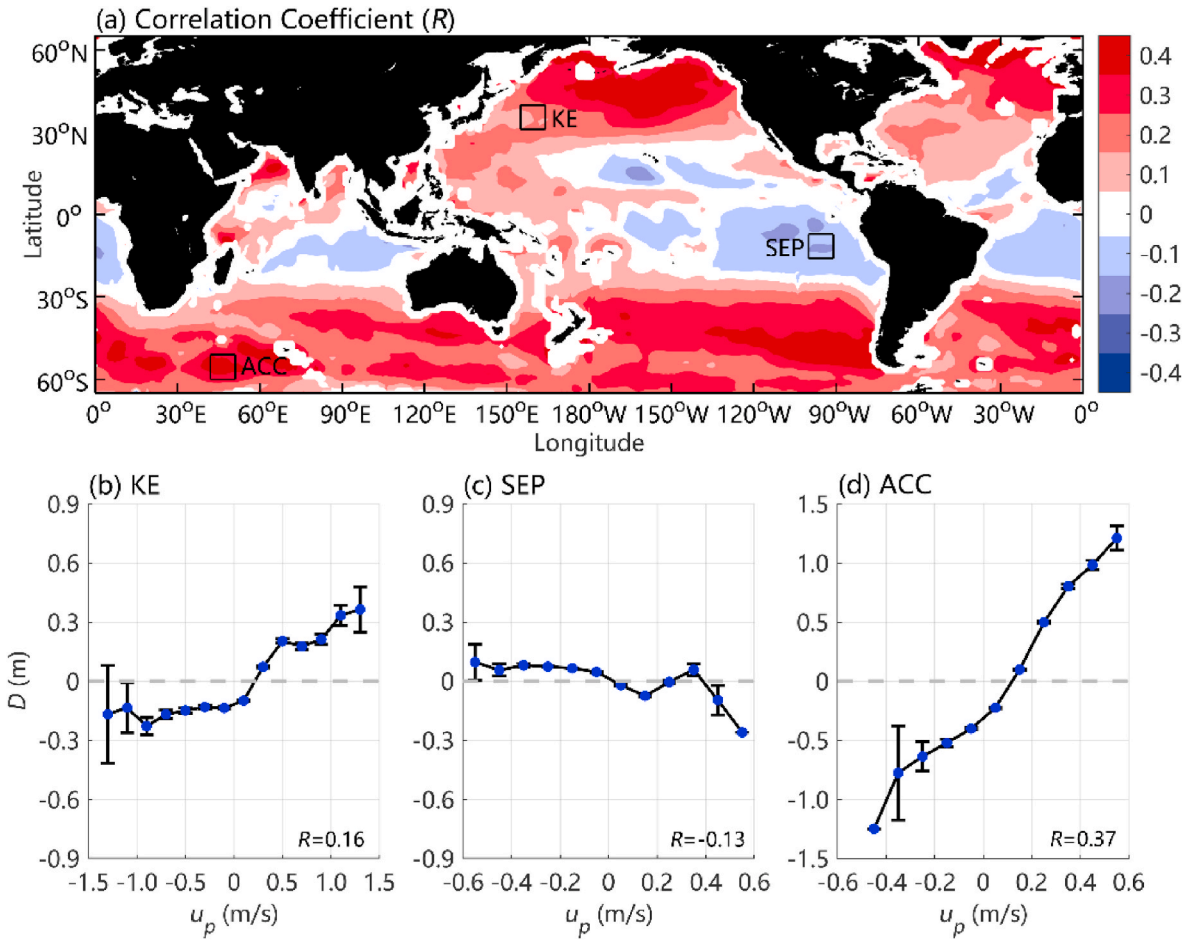

Fig. 8. (a) Linear correlation coefficient (R) between the SWH deviation (D) of GFS-WW3 from altimeter and the projected surface velocities onto wave direction. (b)–(d) Bin-averaged SWH difference (D) as a function of current velocity projections u_p in the KE, Southeast Pacific Ocean, and ACC regions. The bin size is $10^\circ \times 10^\circ$ and the black bars represent the 95% confidence interval of the mean value.

resultant wave height is smaller; if waves and currents oppose each other, the wind stress increases, and so does the momentum flux from wind to waves (Rapizo et al., 2018). The relative wind effect and can be well applied to the stage of wind wave evolution (Ardhuin et al., 2012). However, due to the limitation of the WW3 product, in which the current effects on the wind stress are not involved, the modelled wave height will be definitely biased compared with the real ocean.

To verify the relative wind effect, we replaced the wave direction of WW3 with the wind direction of Global Forecast System, which is the forcing wind field of the WW3 model product, and analyzed the correlation between SWH differences (D) and the angle A between wind direction and current direction (Fig. S4 & Fig. S5). The results are almost the same with our previous findings (Figs. 3 and 5), through with slight errors and lower correlation coefficients. The waves are propagating align to the wind direction in most areas of global ocean, it can be reasonably inferred that the effect of Doppler shift on wave height is amplified by the relative wind effect of surface current, which means that the relative wind effect and the Doppler shift effect of currents make a joint influence on the observed wave height.

Both of the two effects can be explicitly revealed by our observations, which suggest that, without accounting for the effects of ocean currents, approximate 5% of SWH in the simulations are missing or overestimated. However, the two effects are so intertwined that it is difficult to tell them apart in our present analysis. More *in-situ* observations and numerical tests may find a way to this problem.

Except for the local effect of Doppler shift and relative wind, the waves' refraction over currents result in the focusing/defocusing of wave energy, which may influence the wave height not only locally but also down-wave. A numerical modelling study by Ardhuin et al. (2012) has shown that including currents in the model resulted in error reductions by up to 30%, even at locations where current are relatively weak. The influence of refraction on waves is related to the vorticity of the current field (Kenyon, 1971; Dysthe, 2001) and can be well analyzed by combining wave rays' trajectories and the corresponding wave height. However, neither our observations nor the model products have solutions or output of wave directions under the effect of currents, so it is not available to quantify the effect of refraction on wave height under such circumstance. Further studies combining numerical experiments and *in-situ* observations should be conducted to investigate in-depth the non-local effect of ocean currents on waves.

5. Conclusions

By comparing the SWH observed by a fleet of surface drifting wave buoys with GFS-WW3 model product, we provide solid evidences of the modulated wave height by ocean currents. The SWH observed by wave buoys are shown to be generally lower than GFS-WW3 product when the current is roughly aligned with the direction of waves, while it is higher when the current runs against the wave. This feature reveals the Doppler shift effect of ocean surface current on local wave height, although it may be mixed with the impact of relative wind effect. It suggests that the GFS-WW3 product could be underestimated/overestimated approximately by up to 5% of observed SWH if effects of background currents on waves are not involved. Moreover, the deviation of simulated SWH

increases with ocean surface velocities. Further analysis shows the consistent relationship between observed and modelled SWH in the global ocean, except for regions where ocean swells dominate. It implies that the direct effect of currents on wave height is not that prominent in swell-dominant regions.

Considering that many global wind products, which usually force the wave models, are derived from satellite measurements. The wave height simulated by models probably generate substantial errors that should be attributed to 'unreal' winds rather than involvement of wave-current coupling (e.g., Plagge et al., 2012). Therefore, the errors in the simulated wave height may consequently cover up the real wave-current interaction and the associated current-induced wave height variation. In this regard, there are in urgent need for *in-situ* concurrent observations of winds, current and waves in the open oceans to provide more observational evidences and to better uncover the underlying mechanisms.

Based on the conclusion of this study, we can attempt to correct the simulated SWH off-line through the linear relationship between models and observations. This will not increase computational burdens but may provide more accurate model products to the stakeholders like science or shipping communities. However, we remain cautious to expand the relationship investigated in this paper to the studies and applications with different spatial and temporal resolutions.

Declaration of competing interest

The authors declare that they have no known competing financial interests or personal relationships that could have appeared to influence the work reported in this paper.

Acknowledgments

We would like to thank the crew of the R/V Dongfanghong 3, as well as the technicians in Qingdao Haiyan Electronics Co. Ltd for their great efforts. This research is funded by National Natural Science Foundation of China (42076009, 41806009), National Key Research and Development Program of China (2016YFC1402606), Qingdao Pilot National Laboratory for Marine Science and Technology (2017ASTCPES05), Marine S&T Fund of Shandong Province (2018SDKJ0104-5), and Fundamental Research Funds for the Central Universities (201762020). Z. C. is partially supported by the 'Taishan' Scholar Funds (tsqn201812022).

Appendix A. Supplementary data

Supplementary data to this article can be found online at https://doi.org/10.1016/j.dsr.2021.103666.

Data availability statements

The observed data by drifting wave buoys analyzed in this study are publicly available from Figshare repository (doi.org/10.6084/m9.figshare.14498679). The WAVEWATCH III model product are provided by the Pacific Islands Ocean Observing System (PacIOOS, https://www.pacioos.hawaii.edu/metadata/ww3_global.html) for SWH and peak wave direction, and the forcing winds are derived from the Global Forecast System (GFS, https://www.ncei.noaa.gov/products/weather-climate-models/global-forecast). Altimeter data are provided by the Archiving, Validation, and Interpretation of Satellite Data in Oceanography (AVISO, https://www.aviso.altimetry.fr/en/home.html) for SWH. Ocean surface currents are derived from the Hybrid Coordinate Ocean Model (HYCOM, https://www.ncdc.noaa.gov/data-access/model-data/model-datasets/navoceanohycom-glb) and Copernicus-Marine environment monitoring service (CMEMS, https://marine.copernicus.eu/).

References

Ardhuin, F., Gille, S.T., Menemenlis, D., Rocha, C.B., Rascle, N., Chapron, B., et al., 2017. Small-scale open ocean currents have large effects on wind wave heights. J. Geophys. Res.: Oceans 122 (6), 4500–4517. https://doi.org/10.1002/2016JC012413.

Ardhuin, F., Roland, A., Dumas, F., Bennis, A.C., Sentchev, A., Forget, P., et al., 2012. Numerical wave modeling in conditions with strong currents: dissipation, refraction, and relative wind. J. Phys. Oceanogr. 42 (12), 2101–2120. https://doi.org/10.1175/JPO-D-11-0220.1.

Barbariol, F., Benetazzo, A., Carniel, S., Sclavo, M., 2013. Improving the assessment of wave energy resources by means of coupled wave-ocean numerical modeling. Renew. Energy 60, 462–471. https://doi.org/10.1016/j.renene.2013. 05.043.

Benetazzo, A., Carniel, S., Sclavo, M., Bergamasco, A., 2013. Wave–current interaction: effect on the wave field in a semi-enclosed basin. Ocean Model. 70, 152–165. https://doi.org/10.1016/j.ocemod.2012.12.009.

Campos, R.M., D'Agostini, A., França, B.R.L., Cruz, L.M., Soares, C.G., 2021. Extreme wind and wave predictability from operational forecasts at the Drake passage. J. Offshore Mech. Arct. 143 (2) doi. org/10.1115/1.4048151.

Carracedo García, P., Balseiro, C.F., Penabad, E., Gómez, B., Pérez-Muñuzuri, V., 2005. One year validation of wave forecasting at Galician coast. J. Atmos. Ocean Sci. 10 (4), 407–419. https://doi.org/10.1080/17417530601127746.

Chen, G., Chapron, B., Ezraty, R., Vandemark, D., 2002. A global view of swell and wind sea climate in the ocean by satellite altimeter and scatterometer. J. Atmos. Ocean. Technol. 19 (11), 1849–1859. https://doi.org/10.1175/1520-0426(2002)019<1849:AGVOSA>2.0.CO;2.

Craik, A.D., Leibovich, S., 1976. A rational model for Langmuir circulations. J. Fluid Mech. 73 (3), 401–426. https://doi.org/10.1017/S0022112076001420.

Donelan, M.A., Dobson, F.W., Smith, S.D., Anderson, R.J., 1993. On the dependence of sea surface roughness on wave development. J. Phys. Oceanogr. 23 (9), 2143–2149. https://doi.org/10.1175/1520-0485(1993)023<2143:OTDOSS>2.0.CO;2.

Dysthe, K.B., 2001. Refraction of gravity waves by weak current gradients. J. Fluid Mech. 442, 157–159. https://doi.org/10.1017/S0022112001005237.

Fan, Y., Ginis, I., Hara, T., Wright, C.W., Walsh, E.J., 2009. Numerical simulations and observations of surface wave fields under an extremetropical cyclone. J. Phys. Oceanogr. 39 (9), 2097–2116. https://doi.org/10.1175/2009JPO4224.1.

Guimarães, P.V., Ardhuin, F., Sutherland, P., Accensi, M., Hamon, M., Pérignon, Y., et al., 2018. A surface kinematics buoy (SKIB) for wave–current interaction studies. Ocean Sci. 14 (6), 1449–1460. https://doi.org/10.5194/os-14-1449-2018.

Haus, B.K., 2007. Surface current effects on the fetch-limited growth of wave energy. J. Geophys. Res.: Oceans 112 (C3). https://doi.org/10.1029/2006JC003924.

Holthuijsen, L.H., Tolman, H.L., 1991. Effects of the Gulf Stream on ocean waves. J. Geophys. Res.: Oceans 96 (C7), 12755–12771. https://doi.org/10.1029/91JC00901.

Hwang, P.A., 2005. Altimeter measurements of wind and wave modulation by the Kuroshio in the Yellow and East China seas. J. Oceanogr. 61 (5), 987–993. https://doi.org/10.1007/s10872-006-0015-0.

Irvine, D.E., Tilley, D.G., 1989. Ocean wave directional spectra and wave-current interaction in the Agulhas from the Shuttle Imaging Radar-B synthetic aperture radar. J. Geophys. Res. 93 (C12), 15389–15401. https://doi.org/10.1029/JC093iC12p15389.

Jensen, T.G., Rogers, W.E., Gravois, U., Campbell, T., Allard, R., 2011. Wave-current Interaction in the Florida Current in a Coupled Atmosphere-Ocean-Wave Model. OCEANS'11 MTS/IEEE KONA, pp. 1–9. https://doi.org/10.23919/OCEANS.2011.6107015. IEEE.

Kenyon, K.E., 1969. Stokes drift for random gravity waves. J. Geophys. Res. 74 (28), 6991–6994. https://doi.org/10.1029/JC074i028p06991.

Kenyon, K.E., 1971. Wave refraction in ocean currents. Deep Sea Res. Oceanogr. Abstr. 18 (10), 1023–1034. https://doi.org/10.1016/0011-7471(71)90006-4.

Kumar, U.M., Swain, D., Sasamal, S.K., Reddy, N.N., Ramanjappa, T., 2015. Validation of SARAL/AltiKa significant wave height and wind speed observations over the North Indian Ocean. J. Atmos. Sol. Terr. Phys. 135, 174–180. https://doi.org/10.1016/j.jastp.2015.11.003.

Lavrenov, I.V., 1998. The wave energy concentration at the Agulhas current off South Africa. Nat. Hazards 17 (2), 117–127. https://doi.org/10.1023/A:1007978326982.

Liu, A.K., Jackson, F.C., Walsh, E.J., Peng, C.Y., 1989. A case study of wave-current interaction near an oceanic front. J. Geophys. Res. 94 (C11), 16189–16200. https://doi.org/10.1029/JC094iC11p16189.

Longuet-Higgins, M.S., Stewart, R.W., 1961. The changes in amplitude of short gravity waves on steady non-uniform currents. J. Fluid Mech. 10 (4), 529–549. https://doi.org/10.1017/S0022112061000342.

Longuet-Higgins, M.S., Stewart, R.W., 1962. Radiation stress and mass transport in gravity waves, with application to 'surf beats. J. Fluid Mech. 13 (4), 481–504. https://doi.org/10.1017/S0022112062000877.

Mapp, G.R., Welch, C.S., Munday, J.C., 1985. Wave refraction by warm core rings. J. Geophys. Res. 90 (C4), 7153–7162. https://doi.org/10.1029/JC090iC04p07153.

McLeish, W., Ross, D.B., 1985. Wave refraction in an ocean front. J. Geophys. Res. 90 (C6), 11929–11938. https://doi.org/10.1029/JC090iC06p11929.

McWilliams, J.C., Sullivan, P.P., Moeng, C.H., 1997. Langmuir turbulence in the ocean. J. Fluid Mech. 334, 1–30. https://doi.org/10.1017/S0022112096004375.

Meadows, G.A., Shuchman, R.A., Tseng, Y.C., Kasischke, E.S., 1983. SEASAT synthetic aperture radar observations of wave-current and wave-topographic interactions. J. Geophys. Res. 88 (C7), 4393–4406. https://doi.org/10.1029/JC088iC07p04393.

Melville, W.K., Romero, L., Kleiss, J.M., Swift, R.N., 2005. Extreme Wave Events in the Gulf of Tehuantepec, pp. 23–28. Rogue Waves: Proc. 14th 'Aha Huliko 'a Hawaiian Winter Workshop.

Moon, I.J., 2005. Impact of a coupled ocean wave–tide–circulation system on coastal modeling. Ocean Model. 8 (3), 203–236. https://doi.org/10.1016/j.ocemod.2004.02.001.

Osuna, P., Monbaliu, J., 2004. Wave–current interaction in the Southern North Sea. J. Mar. Syst. 52 (1–4), 65–87. https://doi.org/10.1016/j.jmarsys.2004.03.002.

Peregrine, D.H., 1976. Interaction of water waves and currents. Adv. Appl. Mech. 16, 9–117. https://doi.org/10.1016/S0065-2156(08)70087-5.

Plagge, A.M., Vandemark, D., Chapron, B., 2012. Examining the impact of surface currents on satellite scatterometer and altimeter ocean winds. J. Atmos. Ocean. Technol. 29 (12), 1776–1793. https://doi.org/10.1175/JTECH-D-12-00017.1.

Quilfen, Y., Chapron, B., 2019. Ocean surface wave-current signatures from satellite altimeter measurements. Geophys. Res. Lett. 46 (1), 253–261. https://doi.org/10.1029/2018GL081029.

Rapizo, H., Durrant, T.H., Babanin, A.V., 2018. An assessment of the impact of surface currents on wave modeling in the Southern Ocean. Ocean Dynam. 68 (8), 939–955. https://doi.org/10.1007/s10236-018-1171-7.

Rio, M.H., Mulet, S., Picot, N., 2014. Beyond GOCE for the ocean circulation estimate: synergetic use of altimetry, gravimetry, and in situ data provides new insight into geostrophic and Ekman currents. Geophys. Res. Lett. 41 (24), 8918–8925. https://doi.org/10.1002/2014GL061773.

Romero, L., Lenain, L., Melville, W.K., 2017. Observations of surface wave–current interaction. J. Phys. Oceanogr. 47 (3), 615–632. https://doi.org/10.1175/JPO-D-16-0108.1.

Samiksha, V., Vethamony, P., Antony, C., Bhaskaran, P., Nair, B., 2017. Wave–current interaction during Hudhud cyclone in the Bay of Bengal. Nat. Hazards Earth Syst. Sci. 17 (12), 2059–2074. https://doi.org/10.5194/nhess-17-2059-2017.

Stopa, J.E., Cheung, K.F., 2014. Intercomparison of wind and wave data from the ECMWF reanalysis interim and the NCEP climate Forecast system reanalysis. Ocean Model. 75, 65–83. https://doi.org/10.1016/j.ocemod.2013.12.006.

Tamura, H., Waseda, T., Miyazawa, Y., Komatsu, K., 2008. Current-induced modulation of the ocean wave spectrum and the role of nonlinear energy transfer. J. Phys. Oceanogr. 38 (12), 2662–2684. https://doi.org/10.1175/2008JPO4000.1.

Tolman, H.L., 1991. A third-generation model for wind waves on slowly varying, unsteady, and inhomogeneous depths and currents. J. Phys. Oceanogr. 21 (6), 782–797. https://doi.org/10.1175/1520-0485(1991)021<0782:ATGMFW>2.0.CO;2.

Villas Bôas, A.B., Cornuelle, B.D., Mazloff, M.R., Gille, S.T., Ardhuin, F., 2020. Wave–current interactions at meso-and submesoscales: insights from idealized numerical simulations. J. Phys. Oceanogr. 50 (12), 3483–3500. https://doi.org/10.1175/JPO-D-20-0151.1.

Wang, D.W., Liu, A.K., Peng, C.Y., Meindl, E.A., 1994. Wave-current interaction near the Gulf Stream during the surface wave dynamics experiment. J. Geophys. Res.: Oceans 99 (C3), 5065–5079. https://doi.org/10.1029/93JC02714.

Wang, J., Dong, C., Yu, K., 2020. The influences of the Kuroshio on wave characteristics and wave energy distribution in the East China Sea. Deep Sea Res., Part I 158, 103228. https://doi.org/10.1016/j.dsr.2020.103228.

Warner, J.C., Armstrong, B., He, R., Zambon, J.B., 2010. Development of a coupled ocean–atmosphere–wave–sediment transport (COAWST) modeling system. Ocean Model. 35 (3), 230–244. https://doi.org/10.1016/j.ocemod.2010.07.010.

Xie, L., Wu, K., Pietrafesa, L., Zhang, C., 2001. A numerical study of wave-current interaction through surface and bottom stresses: wind-driven circulation in the South Atlantic Bight under uniform winds. J. Geophys. Res.: Oceans 106 (C8), 16841–16855. https://doi.org/10.1029/2000JC000292.

Yang, J., Zhang, J., 2019. Validation of Sentinel-3A/3B satellite altimetry wave heights with buoy and Jason-3 data. Sensors 19 (13), 2914. https://doi.org/10.3390/s19132914.

Yang, J., Zhang, J., Jia, Y., Fan, C., Cui, W., 2020. Validation of Sentinel-3A/3B and Jason-3 altimeter wind speeds and significant wave heights using Buoy and ASCAT data. Rem. Sens. 12 (13), 2079. https://doi.org/10.3390/rs12132079.